

Joint chest X-ray diagnosis and clinical visual attention prediction with multi-stage cooperative learning: enhancing interpretability

Zirui Qiu¹, Hassan Rivaz², and Yiming Xiao¹

¹ Department of Computer Science and Software Engineering, Concordia University, Montreal, Canada

² Department of Electrical and Computer Engineering, Concordia University, Montreal, Canada leoqiuzirui@gmail.com

Abstract. As deep learning has become the state-of-the-art for computer-assisted diagnosis, interpretability of the automatic decisions is crucial for clinical deployment. While various methods were proposed in this domain, visual attention maps of clinicians during radiological screening offer a unique asset to provide important insights and can potentially enhance the quality of computer-assisted diagnosis. With this paper, we introduce a novel deep-learning framework for joint disease diagnosis and prediction of corresponding visual saliency maps for chest X-ray scans. Specifically, we designed a novel dual-encoder multi-task UNet, which leverages both a DenseNet201 backbone and a Residual and Squeeze-and-Excitation block-based encoder to extract diverse features for saliency map prediction, and a multi-scale feature-fusion classifier to perform disease classification. To tackle the issue of asynchronous training schedules of individual tasks in multi-task learning, we proposed a multi-stage cooperative learning strategy, with contrastive learning for feature encoder pretraining to boost performance. Experiments show that our proposed method outperformed existing techniques for chest X-ray diagnosis and the quality of visual saliency map prediction.

Keywords: Computer-Assisted Diagnosis · Visual Attention · X-ray · Explainable AI · Contrastive Learning.

1 Introduction

The continuous advancement of deep learning (DL) in medical imaging has led to a new era in diagnostic radiology, offering diagnostic tools with unprecedented accuracy and efficiency. Particularly in the realm of chest X-ray (CXR) analysis, where the imaging modality has poor soft tissue contrast, DL models have shown significant potential and efficiency in identifying and classifying various pulmonary conditions [6][12]. However, despite their prowess, the black-box nature of many DL-based computer-assisted diagnosis algorithms poses barriers for their clinical adoption, as medical professionals seek not only predictive accuracy, but also transparency and interpretability in automated clinical decisions.

So far, there have been great efforts in explainable AI (XAI) to improve the credence of DL-based diagnostic algorithms. Notably, the flexible Class Activation Map (CAM) [21] and architecture-dependent attention maps from various attention mechanisms (e.g., self-attention [17] and attention gates [16]) have been widely adopted to provide human-attention-like visual interpretations for classification and regression tasks. Nevertheless, their resemblance to the real visual attention of radiologists, which could provide richer insights regarding the diagnostic process, is still limited. Recently, several DL models [10],[24] have been proposed to leverage recorded gaze data as an input or as an auxiliary task to enhance diagnostic accuracy. As gaze data collection requires specialized devices and postprocessing, the latter strategy in a multi-task learning framework appears more attractive in practice. Although multi-task learning could potentially boost the performance of individual tasks in synergy [26], the loss of each task can overfit at different rates if care is not taken, and may limit their performance.

To address the aforementioned challenges, we introduce a novel multi-task DL model based on a cooperative learning strategy to enhance classification performance and clinical visual saliency map prediction simultaneously for chest X-ray. Our contributions are threefold: **First**, to mitigate the issue of asynchronous training schedules of individual tasks, we proposed a multi-stage cooperative learning strategy, which helps with robust training of the designed multi-task network. **Second**, we designed a novel dual-encoder UNet with multi-scale feature-fusion to enhance multi-task collaboration for optimal outcomes. **Lastly**, our experiments demonstrated the superior performance of the proposed method than existing methods, and we share the trained model publicly.

2 Related Works

Public datasets have catalyzed data-driven advancements in chest X-ray image analysis, utilizing networks like ResNet, DenseNet, and EfficientNet for CXR-based disease classification [18]. Besides these advancements, with the potential benefits of enhancing the performance and/or interpretability of relevant DL models, a few groups have directly integrated tracked gaze data during diagnosis into their DL approaches. In GazeRadar, Bhattacharya et al. [1] fused radiomics and visual attention features to perform pulmonary disease classification. Later, the same group [2] proposed RadioTransformer that utilizes visual attention in a cascaded global-focal Transformer framework for CXR classification. Zhu et al. [27] used the visual attention maps to guide the class activation mapping to boost diagnostic accuracy. More recently, Wang et al. [24] proposed GazeGNN, which uses gaze duration to weigh local image features for CXR diagnosis through a graph neural network. Finally, Zhu et al. [26] proposed a multi-task UNet for joint CXR diagnosis and clinical attention map prediction by adopting an elaborate uncertainty-based loss balancing scheme with trainable parameters. In our study, we decided to tackle the challenge with a multi-stage cooperative learning strategy to boost the outcomes further.

3 Methods and Materials

An overview of our proposed technique is illustrated in Fig. 1, which is composed of a dual-encoder residual squeeze-and-excitation UNet (Res_SE-UNet) to predict visual saliency maps, a DenseNet-201 to encode image features, and a classifier module with multi-scale feature-fusion to provide CXR diagnosis. In our cooperative learning framework, these components were trained in three main stages, in the order of the DenseNet-201 feature encoder, residual squeeze-and-excitation UNet, and multi-scale feature-fusion classifier, to allow a gradual introduction of cooperation of the two learning tasks.

3.1 Stage 1: DenseNet-201 Feature Encoder

As DenseNets have shown great performance in image classification tasks, we used the DenseNet-201 as a key feature encoder for the designated tasks. To augment its robustness in feature representation, we first pretrained the network using the CXR data with a contrastive triplet loss [7], which minimizes the distances between similar image pairs while maximizing those between dissimilar ones. Then, the pretrained DenseNet201 was finetuned for the task of classifying a CXR scan into normal, pneumonia, or heart failure, with a cross-entropy loss. Here, we used all layers of the DenseNet-201 before the last dense block as our image feature encoder.

3.2 Stage 2: Visual Saliency Map Prediction

The objective of Stage 2 was to generate a visual saliency map for an input CXR scan that mirrors the attention patterns of medical professionals when diagnosing conditions. Following Stage 1, the feature from the trained DenseNet201 encoder was fed into a modified UNet model at the beginning of its decoding path, together with the compressed feature of the same input image from the UNet’s encoding branch [19]. Note that here, we modified the UNet’s encoder blocks with Residual and Squeeze-and-Excitation (SE) blocks (see Fig. 1) to enhance its robustness and training stability [14]. By leveraging features from two distinct image encoders to extract richer and more nuanced information from the CXR images, we intended to enhance the accuracy of visual saliency map prediction at the decoder end. During training, the DenseNet201 feature encoder was kept frozen, while the Res_SE-UNet was trained using paired CXR images and visual attention maps, and a Kullback–Leibler (KL) divergence loss.

3.3 Stage 3: Multi-Scale Feature-Fusion Classifier

In the final stage, we concatenated the feature from the DenseNet-201 encoder and that from the last upsampling layer of the Res_SE-UNet, and fed them into a simple CNN classifier (Fig. 1) to conduct CXR diagnosis (normal, pneumonia, or heart failure). This enabled full collaboration of two designated tasks. Here, both the DenseNet-201 encoder and Res_SE-UNet were frozen, and only the classifier was trained based on a cross-entropy loss.

3.4 Dataset and Evaluation Metrics

In our study, we used the “chest X-ray dataset with eye-tracking and report dictation” dataset [9] to develop and validate our proposed algorithm. The dataset contains 1083 chest X-ray scans from the MIMIC-CXR dataset [8], with their corresponding diagnostic results (normal, pneumonia, or heart failure), anatomical segmentation, radiologists’ audio with dictation, and finally, additional eye-tracking data collected during radiological diagnosis. The eye-tracking data was obtained with a GP3 gaze tracker by Gazepoint (Vancouver, Canada), with an accuracy of around 1° of visual angle at a sampling rate of 60 Hz. For our study, we utilized the visual saliency maps that represent the gaze location and attention over time as a heat map. As the X-ray images have different resolutions and dimensions, we padded and resampled them to the resolution of 640×512 pixels, and normalized the pixel intensity to $[0,1]$ per image.

For the proposed algorithm and comparison methods, we focus on the accuracy evaluation of CXR diagnosis (classification of normal, pneumonia, or heart failure) and visual saliency map prediction. Specifically, for diagnostic quality, we measured the area under the curve (AUC) metric for multi-class classification [5] and classification accuracy (ACC) for the overall classification performance, as well as AUCs for three individual classes. In terms of visual saliency prediction quality, we adopted the KL divergence, Pearson’s correlation coefficient (PCC), and histogram similarity (HS), which measure the distribution similarity between the predicted and gaze heat maps. While a lower KL divergence is preferred, higher values for the rest of the metrics signify better results. For the metrics that assess the quality of visual saliency map production, two-sided paired sample t-tests were performed to confirm the superiority of our proposed technique against the comparison methods, and a p-value lower than 0.05 was used to declare statistical significance.

3.5 Experimental Setup and Ablation Studies

For our experiment, 100 CXR scans, along with the corresponding labels and visual saliency maps, were randomly selected as a test set while the remaining 983 samples were allocated for training purposes [24]. Our proposed method involved training at different stages, with the steps detailed in Section 3.1 ~ 3.3. For each stage, the training process is conducted over 50 epochs. We utilized the Adam optimizer with its default parameters [11] ($\beta_1 = 0.9$, $\beta_2 = 0.999$, and $\epsilon = 1 \times 10^{-8}$) with a learning rate of 0.0001. Early stopping was employed to avoid overfitting, and model training was performed on a desktop computer with Intel Core i9 CPU, Nvidia GeForce RTX 3090 GPU, and 24GB RAM. To validate the performance of our proposed technique, we compared it against the previously established MT-UNet [26], GazeGNN [24], Inception ResNet v2 [4], and UNet [19] for the two target tasks, using the same training setup as our proposed method.

To help gain further insights into the individual elements of our proposed architecture, we conducted a series of four ablation studies. **First**, to investigate the benefit of adopting Residual and SE blocks in UNet for visual saliency

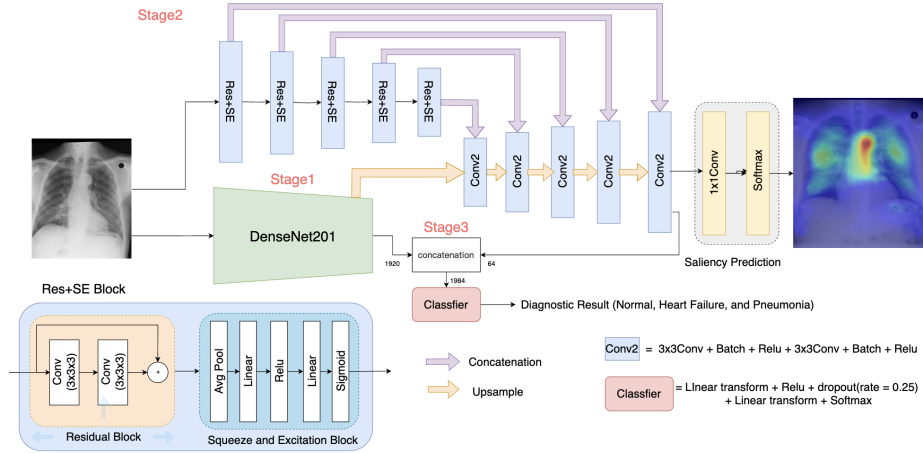


Fig. 1: An overview of the proposed dual-encoder multi-task UNet architecture with multi-stage cooperative learning.

prediction, we compared the heatmap generation quality between only using the Res_SE-UNet and a standard UNet (UNet_S), without the boosting from the DenseNet-201. **Second**, to confirm the contribution of the pretrained DenseNet-201 encoder, we further compared the saliency map prediction accuracy with and without the encoder module (full network vs. Res_SE-UNet). **Third**, the image classification accuracy of full network vs. DenseNet-201 with contrastive learning was investigated to inspect the benefit of multi-scale feature fusion. **Finally**, to reveal the advantage of contrastive learning for pretraining the DenseNet-201, we compared the results with and without contrastive learning pretraining for the network in CXR classification.

4 Results

4.1 Performance of the proposed method

The quantitative accuracy assessments of CXR classification and saliency map prediction for our proposed dual-encoder feature-fusion UNet and the comparison techniques. including the evaluations for ablation study purposes are presented in Tables 1 and 2. The arrows within the tables indicate the desired trends of the associated metrics. Overall, our proposed method has achieved an AUC of 0.925 and an accuracy of 80% for CXR diagnosis, outperforming all the comparison methods, including GazeGNN [24], which ranked as the second best method and uses both the X-ray scan and gaze data as inputs. When looking at the AUC results per class, our method achieved the best score for all class-wise AUCs, except for the category of Normal CXR. In terms of visual saliency prediction, our proposed technique significantly outperformed the MT-UNet and standard

UNet ($p < 0.01$) in all evaluation metrics while reaching better scores on average over our proposed Res_SE-UNet ($p > 0.05$ for CC, $p < 0.01$ for KL and HS). In addition, to qualitatively assess the visual saliency map generation, we present the results from our proposed method, against those produced by the MT-UNet [26], the gradCAM results from the DenseNet-201 component of our proposed DL architecture, and the ground truths. We can see that our proposed method has a higher resemblance to the ground truths while the gradCAM outputs have a large discrepancy from the human gaze pattern.

Table 1: Accuracy assessment of chest X-ray classification for our method, MT-UNet [26], DesenNet201 with contrastive pretraining (DNet201-CL), DesenNet201 (DNet201), Inception ResNet v2 (IRNetv2)[4], and GazeGNN [24].

| Metric | Ours | MT-UNet | DNet201-CL | DNet201 | IRNetv2 | GazeGNN |
|--------------------------------|--------------|---------|------------|--------------|---------|---------|
| AUC (Normal) \uparrow | 0.953 | 0.935 | 0.961 | 0.964 | 0.878 | 0.899 |
| AUC (Heart failure) \uparrow | 0.927 | 0.881 | 0.865 | 0.897 | 0.873 | 0.881 |
| AUC (Pneumonia) \uparrow | 0.894 | 0.687 | 0.859 | 0.849 | 0.602 | 0.823 |
| AUC \uparrow | 0.925 | 0.847 | 0.889 | 0.880 | 0.794 | 0.868 |
| Accuracy \uparrow | 0.800 | 0.640 | 0.750 | 0.690 | 0.600 | 0.730 |

Table 2: Accuracy assessment of visual saliency map prediction (mean \pm std) for our method, MT-UNet [26], UNet with a modified Residual-Squeeze-and-Excitation encoder (Res_SE-UNet), and a standard UNet (UNet_S).

| Metric | Ours | MT-UNet | Res_SE-UNet | UNet_S |
|-----------------|-------------------------------------|-------------------|-------------------|-------------------|
| KL \downarrow | 0.706 \pm 0.183 | 0.747 \pm 0.185 | 0.747 \pm 0.193 | 0.781 \pm 0.202 |
| CC \uparrow | 0.576 \pm 0.113 | 0.545 \pm 0.109 | 0.560 \pm 0.108 | 0.531 \pm 0.109 |
| HS \uparrow | 0.552 \pm 0.055 | 0.535 \pm 0.055 | 0.539 \pm 0.058 | 0.527 \pm 0.056 |

4.2 Ablation studies

We performed four ablation studies for our proposed framework. **First**, when comparing the saliency map generation between the Res_SE-UNet and the standard UNet, we observed a significant improvement in all metrics ($p < 0.05$), indicating the positive impact of SE and residual blocks to better capture task-relevant image features. **Second**, when incorporating the pretrained DenseNet-201 encoder into the Res_SE-UNet to form the dual-encoder setup (i.e., the full model), the quality of visual saliency prediction was further enhanced, with a noticeable drop of KL divergence from 0.747 to 0.706. **Third**, in terms of CXR classification, the full model of our proposed technique was compared against the DenseNet-201 pretrained with contrastive learning, and showed great improvement (Accuracy: 80% vs. 75%). Here, both the second and third studies showcased boosted performance by leveraging the collaboration of the classification

and prediction tasks. **Lastly**, to confirm the benefit of contrastive pretraining for the DenseNet-201 feature encoder, the CXR classification performance of the network with and without CL pretraining were compared in Table 1. With the AUC and accuracy increases of 0.009 and 6%, respectively, the version with CL pretraining is shown to be superior.

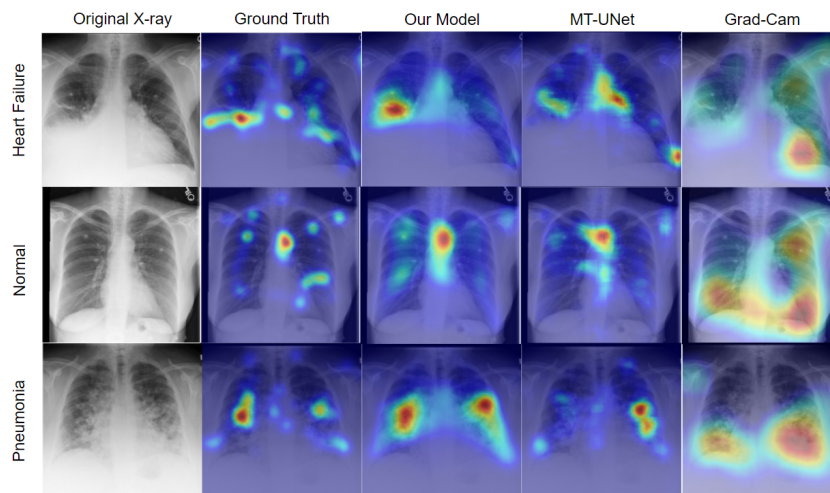


Fig. 2: Qualitative evaluation of visual saliency map prediction across our proposed model and the MT-UNet [26], against the gradCAM outputs from the DenseNet-201 from our proposed model, the original X-ray scan and the ground truths for exemplary heart failure, normal, and pneumonia cases.

5 Discussion

One major feature of our proposed DL framework is to employ a three-stage cooperative learning strategy to address the challenge in multi-task learning, where the loss functions of individual tasks fail to converge at the same rate, resulting in sub-optimal outcomes. Although Zhu et al. [26] successfully demonstrated the adoption of the uncertainty-based training strategy, it requires more elaborate setups and additional learnable parameters to achieve the best outcomes. In contrast, our strategy first used a DenseNet-201 feature encoder pretrained on CXR classification to facilitate visual saliency map prediction, and then further enhance the classification quality by allowing full cooperation of the saliency map and DenseNet-201 features. Based on the ablation studies (see Section 4.2), we showed that such task collaboration with dual-encoder and multi-scale feature-fusion has boosted the performance. In addition, our proposed method outperformed the relatively recent MT-UNet [26] and GazeGNN [24], as well as other baseline techniques in the designated tasks. As in the related reports [26], [24], both MT-UNet and GazeGNN have been validated against several state-of-the-

art DL models, including ResNets, EfficientNet, Swin Transformers, and VGGSSM [3], and showed better results, we decided not to expand the comparison to these models in our study.

In our ablation studies, we confirmed the positive role of contrastive learning with a triplet loss in pretraining the DenseNet-201 feature encoder. Although more recent self-learning techniques have provided better results, they could also be resource demanding. We will further explore these methods in the near future. For saliency map prediction, we proposed the Res.SE-UNet, with Residual and SE blocks. While the SE block can increase feature representation by dynamic channel-wise feature recalibration, the residual block facilitates gradient flow during training. This modification was proven to be instrumental in our method. As the gaze attention during diagnosis reflects the positions and importance of local features relevant to a diagnosis, such information may efficiently guide DL-based algorithms for radiological tasks. In previous investigations [25][20],[13][15], many have confirmed the constructive impacts of incorporating gaze attention maps on improving radiological diagnosis, either as input features with the medical scans or through auxiliary tasks (e.g., regularization of CAM results). This is also well echoed in our study. As shown in Fig. 2, although the highly flexible CAM has been widely used to provide visual explanation for various DL models, in terms of CXR diagnosis, the CAM pattern does not necessarily coincide with real human attentions. Interestingly, in Fig. 2, CAM highlighted the heart for the heart failure case while the human attention focuses on a broader area. Thus, it could be beneficial to employ both visual explanations jointly, and our proposed method can support this option.

In our current study, we utilized the visual attention map, which is an accumulation of temporally sampled gaze locations to provide a potential explanation for the diagnostic results. However, additional representation of the gaze pattern, such as the scanpaths can also be used to enrich the understanding of the diagnostic procedure, identify the skill levels of clinicians to ensure data quality [23], and further enhance the accuracy of the diagnostic algorithm to open doors for additional human-machine-interaction. Although it is still a challenges task and has not been adopted for clinical scans, ongoing scanpath prediction research in natural images [22] is progressing steadily. We will seek to explore venues to incorporate such information in radiological diagnosis in the future.

6 Conclusion

We have proposed a novel multi-task DL model using a dual-encoder UNet with multi-scale feature-fusion for CXR diagnosis and visual saliency prediction. The proposed DL model benefits from our multi-stage cooperative learning strategy to best optimize the training of individual tasks, with a gradual introduction of collaboration. With excellent results, our proposed technique tackles the important challenge of transparency in DL-based radiological diagnosis, with a great potential to be extended for other applications.

Acknowledgment. We acknowledge the support of the Natural Sciences and Engineering Research Council of Canada (NSERC).

References

1. Moinak Bhattacharya, Shubham Jain, and Prateek Prasanna. Gazeradar: A gaze and radiomics-guided disease localization framework. In *International Conference on Medical Image Computing and Computer-Assisted Intervention*, pages 686–696. Springer, 2022. 2
2. Moinak Bhattacharya, Shubham Jain, and Prateek Prasanna. Radiotransformer: a cascaded global-focal transformer for visual attention-guided disease classification. In *European Conference on Computer Vision*, pages 679–698. Springer, 2022. 2
3. Ge Cao, Qing Tang, and Kang-hyun Jo. Aggregated deep saliency prediction by self-attention network. In *Intelligent Computing Methodologies: 16th International Conference, ICIC 2020, Bari, Italy, October 2–5, 2020, Proceedings, Part III 16*, pages 87–97. Springer, 2020. 8
4. Khalid El Asnaoui, Youness Chawki, and Ali Idri. Automated methods for detection and classification pneumonia based on x-ray images using deep learning. In *Artificial intelligence and blockchain for future cybersecurity applications*, pages 257–284. Springer, 2021. 4, 6
5. Tom Fawcett. An introduction to roc analysis. *Pattern recognition letters*, 27(8):861–874, 2006. 4
6. Shimpy Goyal and Rajiv Singh. Detection and classification of lung diseases for pneumonia and covid-19 using machine and deep learning techniques. *Journal of Ambient Intelligence and Humanized Computing*, 14(4):3239–3259, 2023. 1
7. Elad Hoffer and Nir Ailon. Deep metric learning using triplet network. In *Similarity-Based Pattern Recognition: Third International Workshop, SIMBAD 2015, Copenhagen, Denmark, October 12–14, 2015. Proceedings 3*, pages 84–92. Springer, 2015. 3
8. Alistair EW Johnson, Tom J Pollard, Seth J Berkowitz, Nathaniel R Greenbaum, Matthew P Lungren, Chih-ying Deng, Roger G Mark, and Steven Horng. MIMIC-CXR, a de-identified publicly available database of chest radiographs with free-text reports. *Scientific data*, 6(1):317, 2019. 4
9. Alexandros Karargyris, Satyananda Kashyap, Ismini Lourentzou, Joy T Wu, Arjun Sharma, Matthew Tong, Shafiq Abedin, David Beymer, Vandana Mukherjee, Elizabeth A Krupinski, et al. Creation and validation of a chest x-ray dataset with eye-tracking and report dictation for ai development. *Scientific data*, 8(1):92, 2021. 4
10. Sota Kato, Masahiro Oda, Kensaku Mori, Akinobu Shimizu, Yoshito Otake, Masahiro Hashimoto, Toshiaki Akashi, and Kazuhiro Hotta. Classification and visual explanation for covid-19 pneumonia from ct images using triple learning. *Scientific Reports*, 12(1):20840, 2022. 2
11. Diederik P Kingma and Jimmy Ba. Adam: A method for stochastic optimization. *arXiv preprint arXiv:1412.6980*, 2014. 4
12. Paras Lakhani and Baskaran Sundaram. Deep learning at chest radiography: automated classification of pulmonary tuberculosis by using convolutional neural networks. *Radiology*, 284(2):574–582, 2017. 1
13. Ricardo Bigolin Lanfredi, Ambuj Arora, Trafton Drew, Joyce D Schroeder, and Tolga Tasdizen. Comparing radiologists’ gaze and saliency maps generated by interpretability methods for chest x-rays. *arXiv preprint arXiv:2112.11716*, 2021. 8
14. Hao Liu, Jiancheng Luo, Bo Huang, Haiping Yang, Xiaodong Hu, Nan Xu, and Liegang Xia. Building extraction based on se-unet. *Journal of Geo-Information Science*, 2019. 3

15. André Luís, Chihcheng Hsieh, Isabel Blanco Nobre, Sandra Costa Sousa, Anderson Maciel, Joaquim Jorge, and Catarina Moreira. Integrating eye-gaze data into cxdI approaches: A preliminary study. In *2023 IEEE Conference on Virtual Reality and 3D User Interfaces Abstracts and Workshops (VRW)*, pages 196–199. IEEE, 2023. 8
16. Ozan Oktay, Jo Schlemper, Loic Le Folgoc, Matthew Lee, Mattias Heinrich, Kazunari Misawa, Kensaku Mori, Steven McDonagh, Nils Y Hammerla, Bernhard Kainz, et al. Attention u-net: Learning where to look for the pancreas. *arXiv preprint arXiv:1804.03999*, 2018. 2
17. Amirhossein Rasoulia, Soorena Salari, and Yiming Xiao. Weakly supervised intracranial hemorrhage segmentation using head-wise gradient-infused self-attention maps from a swin transformer in categorical learning. *arXiv preprint arXiv:2304.04902*, 2023. 2
18. Vinayakumar Ravi, Harini Narasimhan, Chinmay Chakraborty, and Tuan D Pham. Deep learning-based meta-classifier approach for covid-19 classification using ct scan and chest x-ray images. *Multimedia systems*, 28(4):1401–1415, 2022. 2
19. Olaf Ronneberger, Philipp Fischer, and Thomas Brox. U-net: Convolutional networks for biomedical image segmentation. In *Medical Image Computing and Computer-Assisted Intervention—MICCAI 2015: 18th International Conference, Munich, Germany, October 5–9, 2015, Proceedings, Part III 18*, pages 234–241. Springer, 2015. 3, 4
20. Khaled Saab, Sarah M Hooper, Nimit S Sohoni, Jupinder Parmar, Brian Pogatchnik, Sen Wu, Jared A Dunnmon, Hongyang R Zhang, Daniel Rubin, and Christopher Ré. Observational supervision for medical image classification using gaze data. In *Medical Image Computing and Computer Assisted Intervention—MICCAI 2021: 24th International Conference, Strasbourg, France, September 27–October 1, 2021, Proceedings, Part II 24*, pages 603–614. Springer, 2021. 8
21. Pranav Kumar Seerala and Sridhar Krishnan. Grad-cam-based classification of chest x-ray images of pneumonia patients. In *Advances in Signal Processing and Intelligent Recognition Systems: 6th International Symposium, SIRS 2020, Chennai, India, October 14–17, 2020, Revised Selected Papers 6*, pages 161–174. Springer, 2021. 2
22. Xiangjie Sui, Yuming Fang, Hanwei Zhu, Shiqi Wang, and Zhou Wang. Scandmm: A deep markov model of scanpath prediction for 360° images. In *IEEE Conference on Computer Vision and Pattern Recognition*, 2023. 8
23. Stephen Waite, Arkadij Grigorian, Robert G Alexander, Stephen L Macknik, Marisa Carrasco, David J Heeger, and Susana Martinez-Conde. Analysis of perceptual expertise in radiology—current knowledge and a new perspective. *Frontiers in human neuroscience*, 13:213, 2019. 8
24. Bin Wang, Hongyi Pan, Armstrong Aboah, Zheyuan Zhang, Ahmet Cetin, Drew Torigian, Baris Turkbey, Elizabeth Krupinski, Jayaram Udupa, and Ulas Bagci. Gazegnn: A gaze-guided graph neural network for disease classification. *arXiv preprint arXiv:2305.18221*, 2023. 2, 4, 5, 6, 7
25. Sheng Wang, Xi Ouyang, Tianming Liu, Qian Wang, and Dinggang Shen. Follow my eye: Using gaze to supervise computer-aided diagnosis. *IEEE Transactions on Medical Imaging*, 41(7):1688–1698, 2022. 8
26. Hongzhi Zhu, Robert Rohling, and Septimiu Salcudean. Multi-task unet: Jointly boosting saliency prediction and disease classification on chest x-ray images. *arXiv preprint arXiv:2202.07118*, 2022. 2, 4, 6, 7
27. Hongzhi Zhu, Septimiu Salcudean, and Robert Rohling. Gaze-guided class activation mapping: leveraging human attention for network attention in chest x-rays classification. *arXiv preprint arXiv:2202.07107*, 2022. 2